journal

J. Am. Ceram. Soc., 97 [2] 432–441 (2014)
DOI: 10.1111/jace.12732

First Identification of Rare-Earth Oxide Nucleation in Chalcogenide Glasses and Implications for Fabrication of Mid-Infrared Active Fibers

Zhuoqi Tang,[‡,§] David Furniss,[‡,§] Michael Fay,[¶] Nigel C. Neate,[‖] Yin Cheng,[††] Emma Barney,[‡,§] Lukasz Sojka,[§] Slawomir Sujecki,[§] Trevor M. Benson,[§] and Angela B. Seddon[‡,§,†]

[‡]Mid-Infrared Photonics Group, Faculty of Engineering, University of Nottingham, University Park, Nottingham NG7 2RD, UK

[§]George Green Institute for Electromagnetics Research, Faculty of Engineering, University of Nottingham, University Park, Nottingham NG7 2RD, UK

[¶]Nottingham Nanoscience and Nanotechnology Centre, Faculty of Engineering, University of Nottingham, University Park, Nottingham NG7 2RD, UK

[‖]Wolfson Centre for Advanced Materials, Faculty of Engineering, University of Nottingham, University Park, Nottingham NG7 2RD, UK

[††]College of Physics and Electronic Science, Changsha University of Science & Technology, Changsha 410114, China

Gallium (Ga) helps solubilize rare-earth ions in chalcogenide glasses, but has been found to form the dominant crystallizing selenide phase in bulk glass in our previous work. Here, the crystallization behavior is compared of as-annealed 0–3000 ppmw Dy^{3+}-doped Ge–As–Ga–Se glasses with different Ga levels: $Ge_{16.5}As_{(19-x)}Ga_xSe_{64.5}$ (at.%), for $x = 3$ and 10, named Ga_3 and Ga_{10} glass series, respectively. X-ray diffraction and high-resolution transmission electron microscopy are employed to examine crystals in the bulk of the as-prepared glasses, and the crystalline phase is proved to be the same: Ge-modified, face centered cubic α-Ga_2Se_3. Light scattering of polished glass samples is monitored using Fourier transform spectroscopy. When Ga is decreased from 10 to 3 at.%, the bulk crystallization is dramatically reduced and the optical scattering loss decreases. Surface defects, with a rough topology observed for both series of as-prepared chalcogenide glasses, are demonstrated to comprise Dy, Si, and [O]. For the first time, evidence for the proposed nucleation agent Dy_2O_3 is found inside the bulk of as-prepared glass. This is an important result because rare-earth ions bound in a high phonon–energy oxide local environment are, as a consequence, inactive mid-infrared fluorophores because they undergo preferential nonradiative decay of excited states.

I. Introduction

The chalcogenide glasses can offer great benefit in the mid-infrared (MIR) region due to their unique properties such as optical transparency, low phonon energy, high optical nonlinearity and also, being glasses, they are readily shaped.[1,2] Rare-earth ion–doped chalcogenide glasses are prime candidates for MIR fiber lasers for use beyond 4-μm wavelength, which have not yet been fabricated worldwide,[3–7] but have been modeled.[8–11] Nonfiber crystal lasers operating at 4.3-μm wavelength had been reported.[12,13] According to reports in the literature, the rare-earth ions, dysprosium (Dy^{3+}),[14–17] praseodymium (Pr^{3+}),[18] erbium (Er^{3+}),[19] terbium (Tb^{3+}),[20] samarium (Sm^{3+}),[21] neodymium (Nd^{3+}),[22] thulium (Tm^{3+})[23], and holmium (Ho^{3+})[24] have been successfully doped in chalcogenide glasses. In particular, selenium-based chalcogenide glasses can be transparent at both the pump and lasing wavelengths for MIR lasing and have sufficiently low phonon energy for long wavelength emission, and high refractive indices for high absorption and emission cross sections.[4] Dy^{3+}-doped Ge–As–Ga–Se glasses are ideal candidates for MIR fiber lasers[10,11,25,26] for emission at 4–5 μm wavelength.

If the rare-earth ion dopant facilitates nucleation and crystal growth then shaping the glass to fiber will induce optical scattering loss.[4] Therefore, how to increase the rare-earth ion concentration without paying any penalty of increased devitrification in the fiber is a vital step in the realistic fabrication of a MIR fiber laser.

In our previous research,[27] 0–2000 ppmw Dy^{3+} ($DyCl_3$)-doped $Ge_{16.5}As_9Ga_{10}Se_{64.5}$(at.%) glasses were investigated and crystals found inside the bulk glasses were identified as a modified face centered cubic (*fcc*) α-Ga_2Se_3 with 3 ± 1 substitution of Ge. (It should be noted that we found the same Ge-modified *fcc* α-Ga_2Se_3 phase grew in the fiber of similar glass,[15] as well as bulk of Dy foil-doped glasses after extended heat treatment at fiber-drawing temperatures.[17]) For the as-prepared Dy^{3+}-doped $Ge_{16.5}As_9Ga_{10}Se_{64.5}$ glasses, visible spot defects occurred on surfaces that had been in static contact with the silica glass containment ampoule during melt-quenching and annealing of the chalcogenide glasses.[27] These spot defects contained high concentrations not only of Dy^{3+} but also of Si and [O], indicating contamination passing from the silica glass containment melt–ampoule into the chalcogenide supercooled melt.[27]

It has been proposed[27] that, during glassmelting, the added Dy^{3+}, being the most electropositive species, tends to scavenge oxygen [O], the most electronegative species in the melt, potentially to form Dy_2O_3. [O] in the chalcogenide glassmelt originates from contamination brought in by the glass precursors (as water, hydroxide, and oxide) and from the adjacent silica glassmelting containment (see Section 3.3). Furthermore, it was suggested that Dy_2O_3 can act as a heterogeneous nucleation agent for growth of the modified α-Ga_2Se_3 crystals because they have a similar lattice structure.[27] However, Dy_2O_3 material has not been observed in

J. Ballato—contributing editor

Manuscript No. 33744. Received September 2, 2013; approved October 23, 2013.
†Author to whom correspondence should be addressed. e-mail: angela.seddon@nottingham.ac.uk

bulk glass before. Also, no Dy has been found in the bulk of glasses. However, it should be noted that the Dy doping level was small (≤2000 ppmw) and so if Dy^{3+} ions had instead be homogeneously dispersed in the bulk glass, then Dy would not have been detectable by the methods used.

Although others[28–31] have shown that addition of gallium to sulfide chalcogenide glasses helps to solubilize the rare-earth ions, our previous work[4,15] indicated that decreasing Ga content in Dy^{3+}($DyCl_3$)-doped Ge–As–Ga–Se glasses can give benefit in reducing crystallization and scattering in bulk glasses. This work will present a detailed study of the effect of Ga content on crystallization of selenide-based chalcogenide glasses, both in the bulk glass and at the glass surface. Some new results on the nature of the crystallizing phase will be discussed. Thus, 0–3000 ppmw Dy^{3+}-doped glasses (Dy^{3+} was added as $DyCl_3$) were prepared by the melt-quenching method, with Ga substituted for As and with two different Ga levels: $Ge_{16.5}As_{(19-x)}Ga_xSe_{64.5}$ (at.%), for $x = 10$ and 3; these were named the Ga_{10} and Ga_3 glass series, respectively. The 0–2000 ppmw Dy^{3+} doping and 10 at.% Ga have been fully discussed in our previous work[27] and are taken here as a reference for comparison.

In the present work, the as-annealed Ga_{10} and Ga_3 glass series were investigated for devitrification by means of: X-ray diffraction (XRD), high-resolution transmission electron microscopy (HRTEM), with electron dispersive X-ray spectroscopy (EDX) and selected-area electron diffraction (SAED), and environmental scanning electron microscopy (ESEM), and characterized for light scattering, *via* Fourier transform infrared spectrometry (FTIR).

It was found that when the Ga addition was decreased from 10 to 3 at.%, bulk crystallization dramatically reduced and optical scattering decreased. As stated above, Dy_2O_3 was proposed[27] to act as a heterogeneous nucleation agent for the Ge-modified *fcc* α-Ga_2Se_3 phase due to their close lattice registry. Here, for the first time we present HRTEM evidence for Dy_2O_3 in the bulk of a Ga_3 glass, lying adjacent Ge-modified Ga_2Se_3 crystals, lending support to this hypothesis. This has implications for making a MIR fiber laser, not least because rare-earth ions bound in a high phonon–energy oxide local environment are inactive MIR fluorophores and undergo nonradiative decay of excited states, and so their mid-IR emission rare-earth ion cross sections are compromised.

This work will show the importance of optimizing the Ga at.% for reduction or removal of crystallization and light scattering in bulk glass, such that the maximum rare-earth ion dopant concentration can be achieved without precipitating gallium as the gallium selenide phase. A rationale of the effect of Ga content on the crystallization behavior of rare-earth–doped selenide-based chalcogenide glass should help guide modification in the chalcogenide host glass structure toward avoiding crystallization problems in both rare-earth–doped bulk glasses and fibers for photonic devices, especially MIR fiber lasers. The study also addresses how some of the added Dy is lost to Dy_2O_3.

II. Experimental Procedure

(1) Glassmelting and Annealing

$Ge_{16.5}As_{(19-x)}Ga_xSe_{64.5}$ (at.%), for $x = 10$ and 3 glasses were prepared by the melt-quenching method. High purity host glass elements: Ge (5N; Cerac, Hungerford, UK), As (7N; Furukawa Denshi, KamiYoshima, Japan), Ga (5N; Cerac), and Se (5N; Cerac), together with 500, 800, 900, 1000, 1500 (1550), 2000, or 3000 ppmw Dy^{3+}, added as $DyCl_3$ powder (4N; Sigma-Aldrich, Dorset, UK), were batched into a prior air-baked, and vacuum-baked, silica glass ampoule (<0.1 ppm OH, ID/OD = 10 mm/14 mm; MultiLab, Newcastle, UK) inside a N_2-circulated glove box (≤0.1 ppm O_2, ≤0.1 ppm H_2O; MBraun, Mansfield, UK). The ampoule, containing the chalcogenide glass batch, was sealed under vacuum (~10^{-3} Pa) and experienced 96-h rocking at 930°C in a furnace (TF105/4.5/1ZF; Instron, High Wycombe, UK) to achieve melt homogenization. Subsequently, the furnace temperature was decreased to 800°C and there was a 2-h vertical dwell for refining. The melt was quenched *in situ* through the glass transition temperature (T_g) in a liquid metal alloy pot (Seba Developments Ltd., Keighley, UK) and the ampoule was then placed into a furnace, preset at the T_g, for annealing for 1 h. Then, the furnace and the ampoule slowly cooled to ambient to make chalcogenide glass rod samples, which were each ~8–9 g.

(2) Glass Characterization

(A) XRD: Powdered XRD samples of as-prepared Dy^{3+}-doped Ge–As–Ga–Se glass were put into an Al sample holder and placed in a Siemens (Surrey, UK) Krystalloflex 810 X-ray diffractometer for collection of the XRD pattern, with CuK_α radiation from 10 to 70° 2θ at 2.5 s per step size 0.02.

(B) HRTEM, -SAED, -EDX: To obtain a chalcogenide glass bulk sample for TEM imaging, 3000 ppmw Dy^{3+}-doped $Ge_{16.5}As_{16}Ga_3Se_{64.5}$ glass samples were prepared excluding the surface glass by chipping away the outer surface of a glass disk, which had been sliced from the as-prepared chalcogenide glass rod. The HRTEM samples were placed on a carbon/Cu grid. A JEOL (Tokyo, Japan) 2100F Field Emission gun (FEG)-HRTEM with a Gatan Orius camera was operated for selected-area electron diffraction (HRTEM-SAED) and an Oxford Instruments INCA TEM 250 energy dispersive X-ray spectroscopy (HRTEM-EDX) system was employed to collect TEM-EDX spectra, which exhibited ~±1 at.% accuracy for elements with greater atomic mass than oxygen.

(C) ESEM, -EDX: In the glass surface analysis, the as-prepared chalcogenide glass samples, which had visible spot defects on the surfaces, were imaged and analyzed in an EI XL30 field-emission gun environmental scanning electron microscopy (FEG ESEM). An Oxford Instruments INCA x-sight Si(Li) detector was employed for obtaining the ESEM-EDX results which had approximately ±0.5 at.% accuracy for elements with greater relative atomic mass than oxygen analyzed in this work.

For both the HRTEM-EDX and ESEM-EDX quantification results, because the X-ray energy was low (525 eV), the absorption correction for oxygen could not be accurately determined and so [O] was unquantified.

(D) FTIR: In FTIR measurements, 10 mm diameter, ~2–3 mm thick disk samples were sliced from as-prepared bulk chalcogenide glass rods and carefully ground flat and polished to a 1 μm finish. The FTIR spectral collection was carried out using a FTIR spectrometer system (IFS 66/S; Bruker, Coventry, UK). The circular aperture diameter used inside the sample chamber of the FTIR was 5.0 mm; hence, the surface deposits were avoided because the aperture fitted well within the circumference of the disk samples.

III. Results and Discussion

(1) X-ray Diffraction

As reported earlier[27] for the Ga_{10} glass series (Fig. 1), XRD crystallization peaks appeared at a threshold level of 1000 ppmw Dy^{3+}, identified as the Ge-modified *fcc* α-Ga_2Se_3 and grew in proportion to the added Dy^{3+}, as the Dy^{3+} concentration was increased from 1000 to 2000 ppmw in Ga_{10} glasses (Fig. 2, main peak 28.28° 2θ). However, for the new work here, as the Dy^{3+} concentration was increased further, from 2000 to 3000 ppmw, the XRD peak heights appeared to plateau. Please note that all of the XRD patterns of the Ga_{10} series showed background amorphous humps attributable to the residual glassy matrix, and at zero Dy^{3+} addition, the host glass showed no tendency for crystallization on melt cooling.

To explain the observed behavior, accepting that Dy_2O_3 can nucleate the Ge-modified *fcc* α-Ga_2Se_3 phase due to their

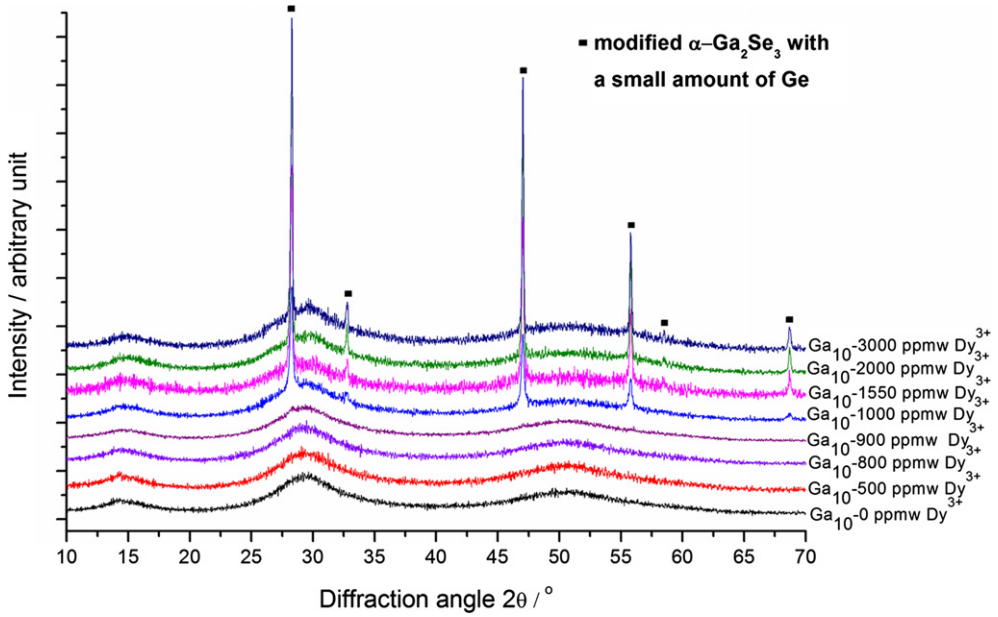

Fig. 1. Powder X-ray diffraction (XRD) patterns of 0–3000 ppmw Dy^{3+}($DyCl_3$)-doped $Ge_{16.5}As_9Ga_{10}Se_{64.5}$ glasses. All of the XRD patterns were $K_{\alpha 2}$ stripped and their background intensity was normalized and vertically shifted to be separated.

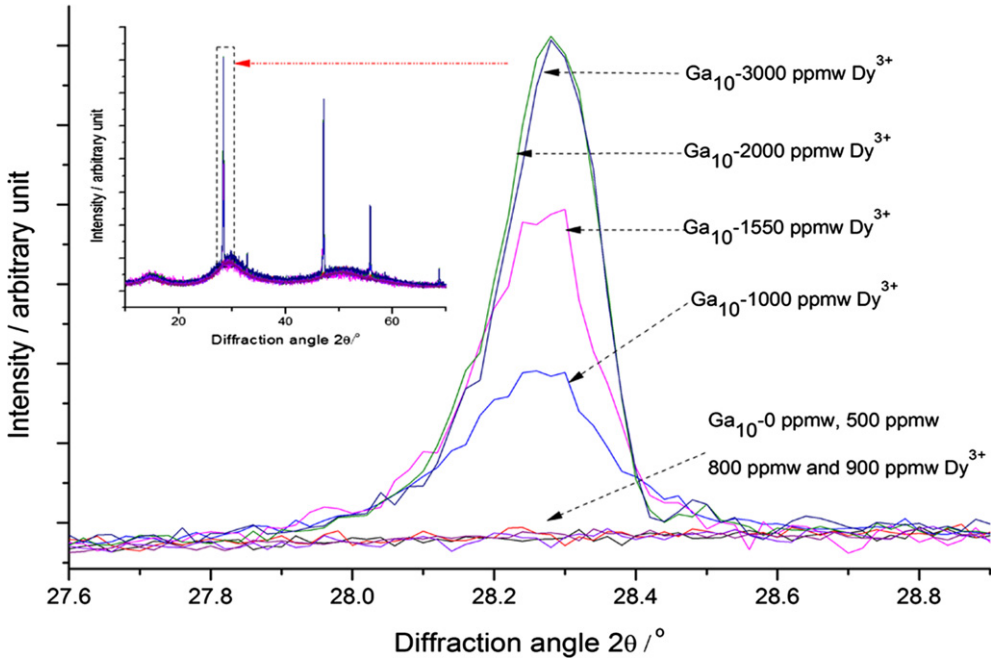

Fig. 2. Relative intensity of the most intense X-ray diffraction peak at 28.28° 2θ of the modified *fcc* α-Ga_2Se_3 phase growing in the 0–3000 ppmw Dy^{3+}($DyCl_3$)-doped $Ge_{16.5}As_9Ga_{10}Se_{64.5}$ glasses, after $K_{\alpha 2}$ stripping and background intensity normalization.

closely matched unit cell dimensions and crystallography,[27] then adding more Dy^{3+} potentially leads to more Dy_2O_3 nucleation sites (assuming adventitious oxide is available), and so greater nucleation of the Ga_2Se_3 phase. For the Ga_{10} series, the apparent lack of continued growth of the modified α-Ga_2Se_3 phase beyond 2000 ppmw added Dy^{3+} might indicate one or more of the following happening in the supercooled melt during the melt cooling:

1. That all of the added Ga had crystallized to the modified α-Ga_2Se_3 phase already at 2000 ppmw Dy^{3+}, so adding more Dy^{3+} could not nucleate more modified α-Ga_2Se_3; that is, only Ge–As–Se was present in the residual glassy matrix and there was no more Ga in the supercooled amorphous phase to crystallize out; the evidence against this is that Ga was found present in the glassy phase for the 2000 ppmw Dy^{3+}-doped Ga_{10} glass in our experiments;
2. That 2000 ppmw Dy^{3+} was the limit of added Dy^{3+} to be able to be oxidized to the supposed Dy_2O_3 nucleation agent, implying a limit of available adventitious [O] to oxidize Dy^{3+}; the evidence against this is the presence of limitless [O] present as SiO_2 in the silica ampoule;
3. That, with a fixed Ga content in the glass, no matter the availability of Dy_2O_3 nucleating sites, the modified α-Ga_2Se_3 phase stops growing at some *quasi*-equilibrium of Ga distributed between the crystal and supercooled melt.

For the Ga_3 glass series, XRD patterns of 0–3000 ppmw Dy^{3+}-doped glasses are given in Fig. 3, together with

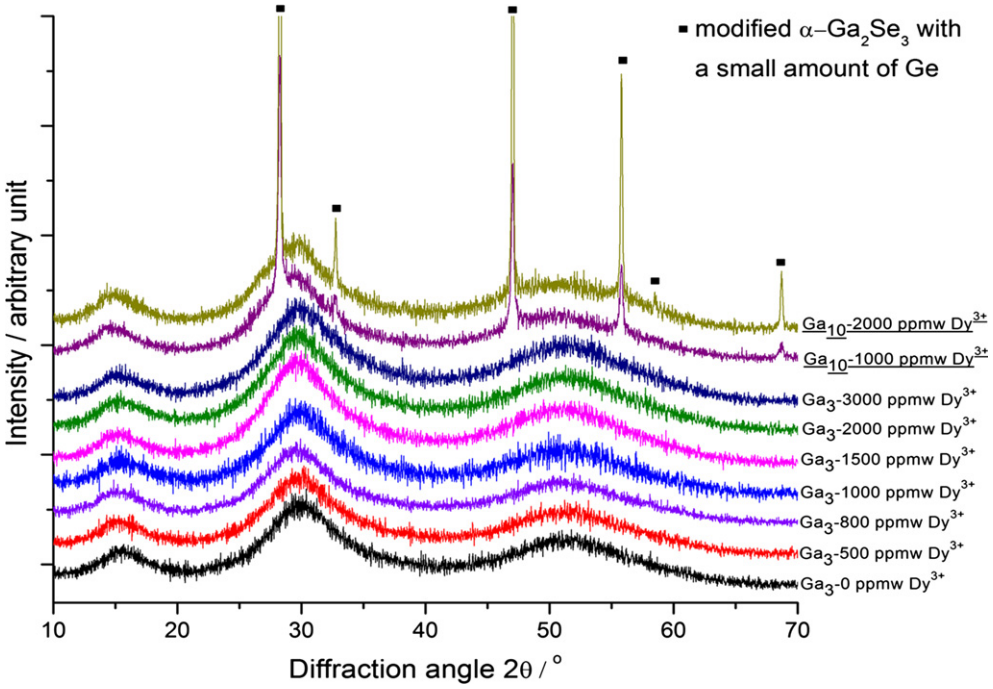

Fig. 3. Powder X-ray diffraction (XRD) patterns of the 0–3000 ppmw Dy^{3+}($DyCl_3$)-doped $Ge_{16.5}As_{16}Ga_3Se_{64.5}$ glasses, and the 1000 and 2000 ppmw Dy^{3+}($DyCl_3$)-doped $Ge_{16.5}As_9Ga_{10}Se_{64.5}$ glasses as reference. (Note all XRD patterns were $K_{\alpha 2}$ stripped, their background intensity was normalized and they were vertically shifted for clarity).

reference Ga_{10} glass series patterns: 1000 and 2000 ppmw Dy^{3+}. In stark contrast to the Ga_{10} series of glasses, where crystals appeared at 1000 ppmw Dy^{3+}, all of the Dy^{3+}-doped Ga_3 series of glasses were X-ray amorphous. This suggests that when the Ga content was decreased from 10 to 3 at.%, Ga remained dissolved in the supercooled Ge–As–Ga–Se glassmelt, and in solid solution in the resulting Ge–As–Ga–Se glass matrix once below the glass transition (T_g), even at the higher Dy^{3+} doping levels and in the possible presence of Dy_2O_3 nucleation sites.

In summary, according to XRD, lowering the Ga content from 10 to 3 at.% dramatically decreased the crystallization on melt cooling of Dy^{3+}($DyCl_3$)-doped Ge–As–Ga–Se glasses.

(2) Transmission Electron Microscopy Study of Nucleation Agent

It is generally accepted that XRD sensitivity is limited to detection of 1–5 vol% of a crystalline phase in an amorphous matrix. Therefore, the amorphous XRD patterns in Fig. 3 are not conclusive evidence for no crystals in the Dy^{3+}-doped Ga_3 series of chalcogenide glasses. In our previous work,[27] a typical 300 nm × 200 nm crystal found inside 2000 ppmw Dy^{3+}-doped Ga_{10} bulk glass was identified, using imaging and analytical HRTEM, to be the Ge-modified *fcc* α-Ga_2Se_3 phase.

In the current work, HRTEM imaging was applied to the bulk of as-prepared 3000 ppmw Dy^{3+}($DyCl_3$)-doped Ga_3 glasses and the great majority of the sampling revealed a single-phase, amorphous glass matrix and no crystals. Figure 4 shows an image of an isolated cluster of nanocrystals (diameter range: ~20–150 nm) found inside the bulk of an as-annealed 3000 ppmw Dy^{3+}($DyCl_3$)-doped Ga_3 glass sample; HRTEM-SAED (inset Fig. 4) confirmed that the nanocrystals exhibited an ordered lattice. The inset HRTEM-EDX spectrum is typical of one of these crystals (see dashed box; size: >100 nm × 100 nm) imaged in Fig. 4 and reveals peaks due to the host glass elements Ge, Ga, and Se but not of As, Dy, Cl, or Si; the Cu peak was the sample holder.

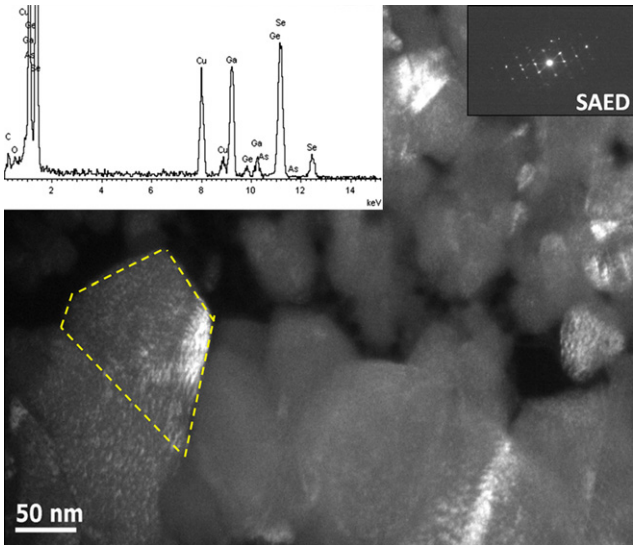

Fig. 4. High-resolution transmission electron microscopy (HRTEM) image of nanocrystals (size: ~20–150 nm) inside the bulk of 3000 ppmw Dy^{3+}($DyCl_3$)-doped $Ge_{16.5}As_{16}Ga_3Se_{64.5}$ glass. The selected-area electron diffraction result (top right inset) proves the crystalline phase. The HRTEM-EDX spectrum of a crystal (see dashed box; size: >100 nm × 100 nm) is presented in the top left inset. The quantified HRTEM-EDX results are given in Table I.

The HRTEM-EDX quantification of elemental composition (Table I) of the crystal (enclosed by the dashed box in Fig. 4; size: >100 nm × 100 nm) gave $Ge_{2\pm1}As_0Ga_{41\pm1}Se_{57\pm1}$ (at.%) which is very close to the stoichiometry of Ga_2Se_3 and is different from the glass batched value of $Ge_{16.5}As_{16.0}Ga_{3.0}Se_{64.5}$. Because the amount of As in the crystal was 0 at.%, instead of the 16.0 at.% expected in the as-batched glass, none of the surrounding glassy area was believed to be overlapped with the crystal during the measurement. This result supports our earlier conclusion[27] that there is a small amount of Ge, there measured at 3 ± 1 at.%

and here at 2 ± 1 at.%, in the α-$GaSe_3$ crystal unit cell. Thus, the HRTEM results indicate that the elemental composition of the crystals in the 3000 ppmw Dy^{3+}($DyCl_3$)-doped Ga_3 glass was close to that of the crystals found in our earlier work in the bulk of the as-prepared 2000 ppmw Dy^{3+}-doped Ga_{10} glass (which was $Ge_{3\pm1}As_0$ $Ga_{38\pm1}Se_{59\pm1}$[27]). It is concluded from the present results that the nature of the crystal phase found in the bulk of the as-prepared glasses of both the Dy^{3+}($DyCl_3$)-doped Ga_3 series and the Ga_{10} series was the same, and was the Ge-modified *fcc* α-Ga_2Se_3, but that the occurrence in equivalently Dy^{3+}-doped glasses was very much lower for the Ga_3 glass series.

In our previous work,[27] although Dy_2O_3 was proposed as a heterogeneous nucleating agent for the modified α-Ga_2Se_3 crystals grown inside the bulk Ga_{10} glass, no direct evidence of Dy was discovered in the bulk of the glass.

Here, the mystery is resolved. An atypical region imaged within the 3000 ppmw Dy^{3+}($DyCl_3$)-doped Ga_3 glass by HRTEM was analyzed in two ways.

First, a HRTEM-EDX spectrum of the whole region imaged in Fig. 5 (named the "area-spectrum") is presented in Fig. 6(a) and shows that the characteristic peak of Dy was observed, accompanied by peaks of the host glass elements: Ge, As, Ga, and Se. The HRTEM-EDX quantification (Table II) of the area spectrum [Fig. 6(a), i.e., the result of the mean of many scanned point spectra in this area] shows that there was 4 ± 1 wt% Dy, compared to that originally batched of 0.3 wt% Dy. Moreover, the observed Ga was 28 ± 1 at.% (batched 3.0 at.%) and Se was 60 ± 1 at.% (batched 64.5 at.%) giving Ga:Se≈1:2, which indicates the probable presence of Ge-modified *fcc* α-Ga_2Se_3 (Ga:Se = ~1:1.4) crystals in this same region. The measured As was 2 ± 1 at.% (batched 16.0 at.%) and not zero% as expected for phase-pure Ge-modified α-Ga_2Se_3, which suggests that a small amount of glassy material overlapped during the HRTEM-EDX area-spectral measurement accounting for the measured Ga:Se stoichiometry (~1:2) not exactly matching that of the Ge-modified Ga_2Se_3 (~1:1.4). Ge (observed 8 ± 1 at.%, batched 16.5 at.%) was correspondingly decreased from the as-batched value yet greater than 2 ± 1 at.%, expected for the Ge-modified *fcc* α-Ga_2Se_3, reaffirming that there was overlap with the parent glass during the HRTEM-EDX area-spectrum measurement. Finally, discussion of Fig. 4 shows that the crystallization of Ge-modified Ga_2Se_3 was likely. Therefore, we have demonstrated, by means of the HRTEM-EDX area spectrum [Fig. 6(a)] that Dy was found in, likely, a Ge-modified α-Ga_2Se_3 crystal-rich region (Fig. 5). EDX does not measure oxidation state of elements, but we can say that probably this Dy was present as Dy^{3+} as it was batched as Dy^{3+} (in $DyCl_3$) and had no redox possibility of reduction to Dy^0 in this anion-rich glass formulation (average coordination number $\langle r \rangle = 2.52$, where $\langle r \rangle = 2.40$ for stoichiometry[32]).

Secondly, HRTEM-EDX point analyses were conducted. In contrast to the HRTEM-EDX area spectrum, a HRTEM-EDX

Table I. Quantification of Elemental Composition Based on the HRTEM-EDX Spectrum Shown for the Crystal (Dashed Line; Size: >100 nm × 100 nm) in Fig. 4 for 3000 ppmw Dy^{3+}($DyCl_3$)-Doped $Ge_{16.5}As_{16}Ga_3Se_{64.5}$ Glass

Element	Ge	As	Ga	Se
Material batched/at.%	16.5	16.0	3.0	64.5
HRTEM-EDX observed/at.%	2 ± 1	0 (±1)	41 ± 1	57 ± 1
Ga_2Se_3 (Theory)/at.%	—	—	40	60

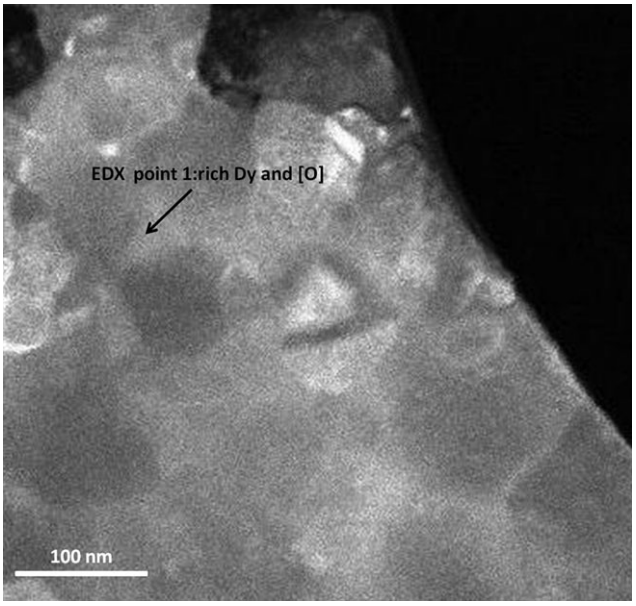

Fig. 5. High-resolution transmission electron microscopy image of suggested Dy_2O_3 nucleating agents found in rich Ga area inside the bulk of 3000 ppmw Dy^{3+}($DyCl_3$)-doped $Ge_{16.5}As_{16}Ga_3Se_{64.5}$ glass. The EDX spectra are shown in Fig. 6 and the corresponding quantified composition is given in Table II.

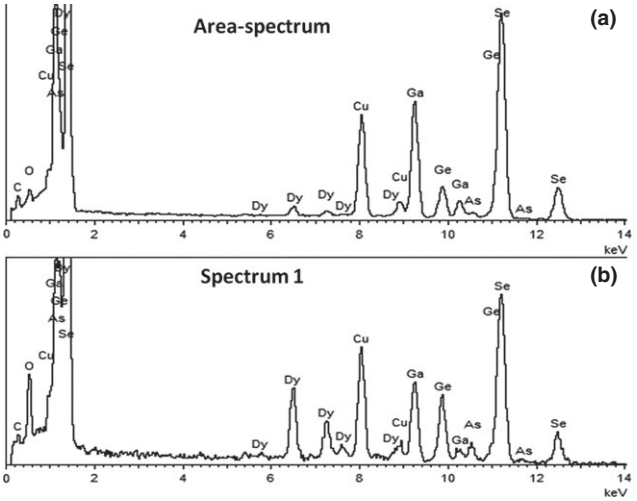

Fig. 6. HRTEM-EDX acquired: (a) area spectrum and (b) point spectrum 1, both from in the bulk of a sample of the 3000 ppmw Dy^{3+}($DyCl_3$)-doped $Ge_{16.5}As_{16}Ga_3Se_{64.5}$ glass, imaged in Fig. 5. Area spectrum means the HRTEM-EDX spectrum of the whole region shown in Fig. 5, whereas that acquired at a higher resolution to the HRTEM beam itself is referred to as point spectrum 1. The quantified HRTEM-EDX composition results are in Table II.

Table II. Quantification of the Compositions Associated with the HRTEM-EDX Spectra in Fig. 6 (of HRTEM Image in Fig. 5) for 3000 ppmw Dy^{3+}($DyCl_3$)-Doped $Ge_{16.5}As_{16}Ga_3Se_{64.5}$ Glass. The HRTEM-EDX Spectrum of the whole Region Shown in Fig. 5 is Referred to as the "Area-spectrum" as Opposed to the High-Resolution Point Spectrum 1 within the Same Region of Fig. 5 to Demonstrate the Very High Level of Dy Found for this Particular Point Spectrum

Element	Ge/at.%	As/at.%	Ga/at.%	Se/at.%	Dy/wt%
Material batched	16.5	16.0	3.0	64.5	0.3
Area spectrum	8 ± 1	2 ± 1	28 ± 1	60 ± 1	4 ± 1
Point spectrum 1	15 ± 1	4 ± 1	19 ± 1	48 ± 1	27 ± 1

point spectrum was collected over a very small nm-scale region of the same order of resolution as that the HRTEM beam diameter itself, which was nominally 1 nm and the majority of the intensity of the beam was 1 nm diameter at the sample with faint spreading to 10 nm diameter. One of the HRTEM-EDX point-spectral results was selected for presentation here [HRTEM-EDX point spectrum 1, Fig. 6(b)], which was acquired from within the region highlighted in Fig. 5. This point spectrum 1 illustrates an area exceedingly Dy rich: 27 ± 1 wt% Dy (Table II), *c.f.* as-batched was 0.3 wt% Dy. Now, the Dy peak of the HRTEM-EDX point spectrum 1 [Fig. 6(b)] is far larger than the Dy peak of the HRTEM-EDX area spectrum [Fig. 6(a)], and, moreover, is accompanied by a concomitant rise in intensity of the [O] peak. Although the oxygen level cannot be quantified here, we propose nevertheless that the concomitant increase in both Dy and [O] is good evidence for their chemical association as Dy_2O_3. SAED of the same area showed both crystalline and glassy nature and was not conclusive. Note, no silicon was found in the vicinity [Figs. 5, 6(a) and (b)]; silicon was found neither in the bulk of the Ga_3 glass series nor Ga_{10} glass series.[27]

In our earlier work, Dy_2O_3 was proposed as a heterogeneous nucleating agent for the Ge-modified α-Ga_2Se_3 phase,[27] given their close unit cell lattice match: both cubic with Dy_2O_3 double lattice parameter of the Ge-modified α-Ga_2Se_3. Here, the quantification (Table II), of the HRTEM-EDX point spectrum 1 [Fig. 6(b)], of the crystalline region depicted in Fig. 5, yields host glass elements in ratio: $Ge_{15\pm1}As_{4\pm1}Ga_{19\pm1}Se_{48\pm1}$ (at.%) which, when compared to the originally batched composition: $Ge_{16.5}As_{16.0}Ga_{3.0}Se_{64.5}$ (at.%), indicates a Ga-rich region in the vicinity of the detected Dy-[O] region. Therefore, it is tentatively concluded, from the high-resolution point-spectral measurements, that Ge-modified α-Ga_2Se_3 lies here in juxtaposition with the Dy_2O_3.

To summarize, direct evidence from HRTEM has been presented, for the first time, to support the proposal of Dy_2O_3 heterogeneous nucleation of Ge-modified *fcc* α-Ga_2Se_3 crystals observed within the bulk of a 3000 ppmw Dy^{3+}-doped as-prepared Ga_3 glass. Particulate Dy_2O_3 in the as-prepared glasses is a strong source of light scattering, and this is discussed further in Section 3.4.

(3) Studies of Spot Defects on as-Prepared Chalcogenide Glass Surfaces

Photographs of the as-annealed surfaces of the 2000 and 3000 ppmw Dy^{3+}($DyCl_3$)-doped Ga_3 glasses [Figs. 7(b) and (c), respectively] show surface problems of roughened areas of spot defects clearly visible to the naked eye and of the order hundreds of micrometeres in size, in direct contrast to the submicrometer, bulk crystals discussed in the last Section 3.2. Similar problems were reported previously for Ga_{10} glasses (for ≤2000 ppmw Dy^{3+} (added as $DyCl_3$) doping[27]) and a typical image of the 2000 ppmw Dy^{3+}($DyCl_3$)-doped Ga_{10} glass is given in Fig. 7(a) for comparison.[27]

For both the Ga_{10} and Ga_3 glass series, the roughened-surface spot defects only occurred at chalcogenide glass surfaces which had been in direct contact with the silica glass containment during the static melt cooling and annealing. Note that no distinct surface spot defects could be found on the 500 ppmw Dy^{3+} ($DyCl_3$) doped, and host, Ga_3 and Ga_{10} glasses. When comparing the results of the Ga_3 and Ga_{10} glasses each batched with 2000 ppmw Dy^{3+} [Figs. 7(a) and (b)], the spot defects were of bigger size, on the surface of the Ga_{10} glass than on the Ga_3 glass, although it is difficult to judge the comparative number of defects. This indicates that the decrease in Ga, from Ga_{10} to Ga_3, has led to an improvement of surface integrity for the as-annealed Ga_3 glass. This improvement may be associated with the decreased tendency for devitrification to α-Ga_2Se_3 of the Ga_3 glasses comparing to the Ga_{10} glasses.

On the other hand, for the Ga_3 glasses: when the Dy^{3+} concentration was increased from 2000 ppmw [Fig. 7(b)] to 3000 ppmw [Fig. 7(c)], bigger spot defects were found. Similar behavior of worsening surface quality with increased addition of Dy^{3+} due to similar spot defects was found earlier for the Ga_{10} glass series.[27]

In our previous work[27] on the Dy^{3+}($DyCl_3$)-doped Ga_{10} glasses, surface spot defects were found to consist of Dy, Si, and [O]. For the Ga_3 series glasses here, although the bulk crystallization was hugely decreased (Section 3.1), similar surface problems of spot defects were observed for Ga_3 glasses [Figs. 7(b) and (c)]. Figure 8(a) shows an ESEM image of an affected area of around 300 μm × 300 μm on the surface of the 2000 ppmw Dy^{3+}($DyCl_3$)-doped Ga_3 glass. In Fig. 9, the ESEM-EDX elemental mapping of this area shows the presence of: Si, [O], Dy, and Cl in the area imaged in Fig. 8(a) (but note Cl was not always found with the other three elements). It is concluded that the same type of spot defects were found on the surface of the as-prepared Ga_3 glasses, with characteristically high concentration of Dy, Si, and [O], as found previously for the as-prepared Ga_{10} glass,[27] implying rare-earth ion attack of the silica ampoule during melt cooling and perhaps similar attack during glassmelting.

Furthermore, the ESEM-EDX spectrum 1 [Fig. 8(b)], and its quantification of elemental composition (Table III) of the boxed 100 μm × 100 μm area highlighted in Fig. 8(a), reveals an area rich in Dy, Si, Cl, and [O]; thus, 32.6 ± 0.5 wt% Dy (added to batch: 0.20 wt%), 14.3 ± 0.5 at.% Si (added to batch: zero at.%), 2.9 ± 0.5 wt% Cl (added to batch: 0.13 wt %), and [O] unquantified but >0 at.% (added to batch: zero at.%). Reduced proportions of all the host glass elements composition $Ge_{11.9\pm0.5}As_{10.5\pm0.5}Ga_{2.4\pm0.5}Se_{37.7\pm0.5}$ (added: $Ge_{16.5}As_{16.0}Ga_{3.0}Se_{64.5}$) were also found in this same 100 μm × 100 μm region.

In Fig. 8(a), the marked crossed point, glassy area, near to the boxed spot defect area, was analyzed to give ESEM-EDX spectrum 2 [Fig. 8(c)], which shows that this glassy area was uncontaminated by Dy and Si. The tiny [O] peak is suggested due to chalcogenide glass surface oxidation from ambient storage, which would evenly distribute on the chalcogenide

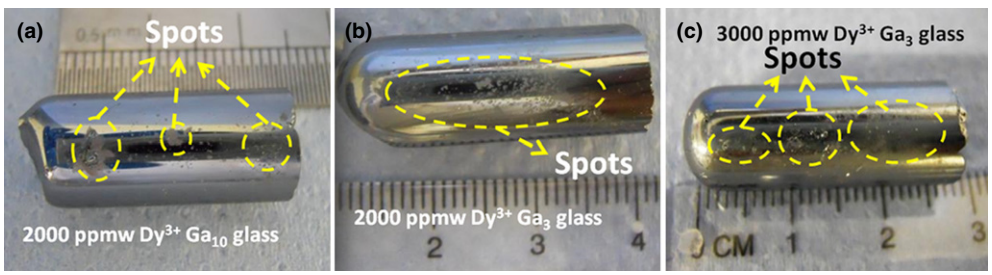

Fig. 7. As-prepared glassmelting results of: (a) 2000 ppmw Dy^{3+}($DyCl_3$)-doped $Ge_{16.5}As_9Ga_{10}Se_{64.5}$ glass; (b) and (c): 2000 and 3000 ppmw Dy^{3+}($DyCl_3$)-doped $Ge_{16.5}As_{16}Ga_3Se_{64.5}$ glass, respectively, showing spot defects at the glass surfaces which had been in contact with the silica glass containment during melt cooling and annealing.

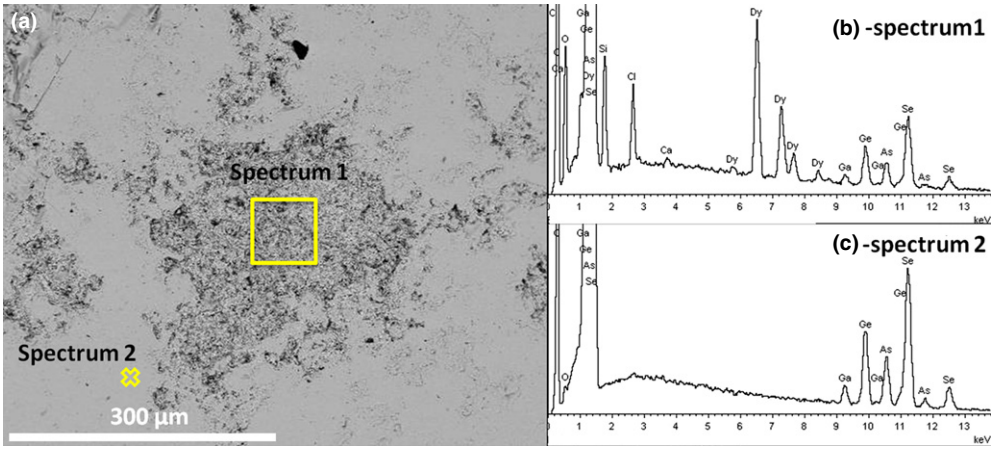

Fig. 8. (a) Environmental scanning electron microscopy (ESEM) image of Dy contaminated surface spot defects of the 2000 ppmw Dy^{3+}($DyCl_3$)-doped $Ge_{16.5}As_{16}Ga_3Se_{64.5}$ glass; (b) ESEM-EDX spectrum 1 of the marked square area in (a); (c) ESEM-EDX spectrum 2 of the marked cross-point on the glassy area in (a). Corresponding quantification of compositions is shown in Table III. ESEM-EDX mapping of (a) is shown in Fig. 9.

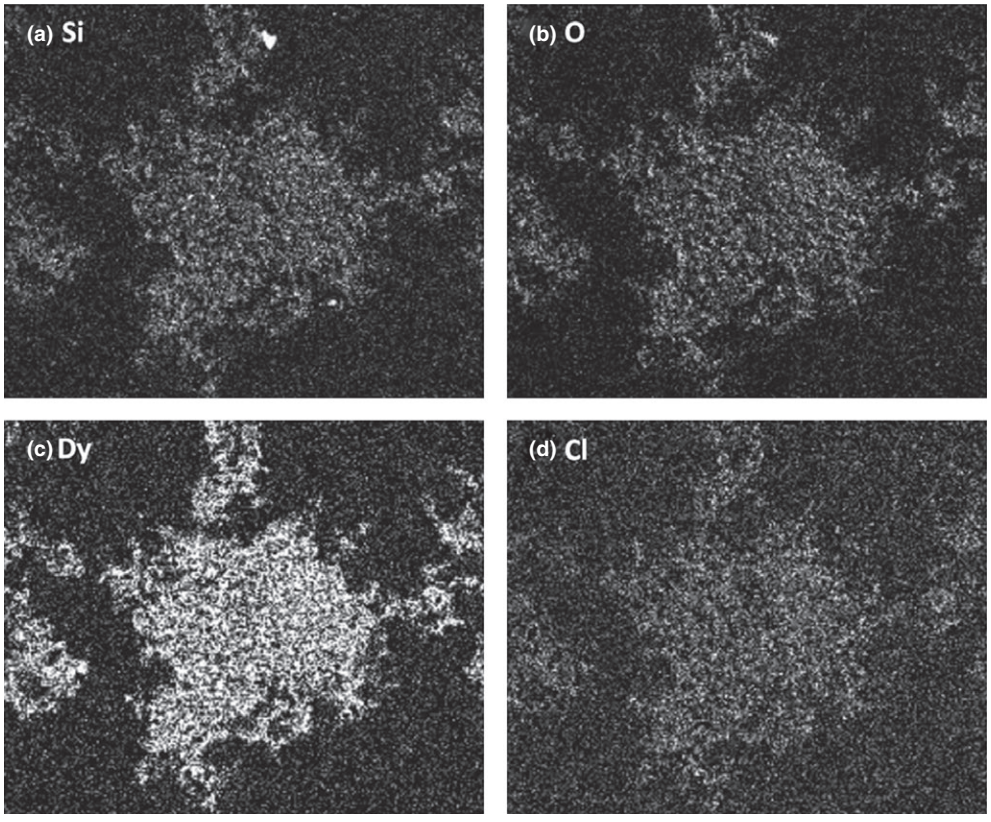

Fig. 9. ESEM-EDX elemental mapping results of the same affected region in Fig. 8(a) of the 2000 ppmw Dy^{3+}($DyCl_3$)-doped $Ge_{16.5}As_{16}Ga_3Se_{64.5}$ glass showing the presence of: (a) Si; (b) [O]; (c) Dy and (d) Cl.

glass surface.[33] ESEM-EDX spectrum 2 [Fig. 8(c)], quantified in Table III, shows that the host element composition of the glassy area of $Ge_{16.9\pm0.5}As_{16.6\pm0.5}Ga_{3.4\pm0.5}Se_{63.1\pm0.5}$ is remarkably close to the as-batched glass composition: $Ge_{16.5}As_{16}Ga_3Se_{64.5}$. This suggests that during the melt quenching, the roughened areas of spot defect on the surfaces of the glass did not affect the composition of adjacent glassy areas on the surfaces of the Dy^{3+}($DyCl_3$)-doped Ga_3 glasses.

In summary, the roughened chalcogenide glass surfaces [Fig. 8(a)] were found to contain high levels of Dy, Si, and [O] by means of ESEM-EDX. The physical shape of the features suggests that the chalcogenide boule surfaces had stuck to the silica glass wall of the ampoule during removal of the selenide glass boule after annealing. As noted previously,[27] the presence of high levels of Si and [O] together in the surface spots must have originated from the silica glassmelting ampoule. We suggest that the mechanism is physical incorporation of corrosion of the ampoule as we have found that simply heating $DyCl_3$ inside an evacuated silica glass ampoule cause attack of the internal ampoule wall in contact with the $DyCl_3$.

(4) Fourier Transform Infrared Spectroscopy Studies

Figures 10 and 11 show the FTIR spectra of samples of 0–3000 ppmw Dy^{3+}-doped for each of the Ga_{10} glass series (including 0–2000 ppmw Dy^{3+}-doped Ga_{10} FTIR spectra from earlier work,[27] for comparison) and Ga_3 glass series

Table III. ESEM-EDX Quantification of Composition of the Boxed, Affected-Area and the Marked Crossed-Point of Glassy Area in Fig. 8(a) for 2000 ppmw Dy^{3+}($DyCl_3$)-Doped $Ge_{16.5}As_{16}Ga_3Se_{64.5}$ Glass. [see also the ESEM-EDX Spectra in Figs. 8(b) and (c)]. Note, the Error of ESEM-EDX is ±0.5 on both at.% and wt% Values

Element	Ge/ at.%	As/ at.%	Ga/ at.%	Se/ at.%	Dy/ wt%	Si/ at.%	Cl/ wt.%	Ca/ at.%
Batched	16.5	16.0	3.0	64.5	0.20	0.0	0.13	0.0
EDX result (rough area)	11.9	10.5	2.4	37.7	32.6	14.3	2.9	0.5
EDX result (glassy area)	16.9	16.6	3.4	63.1	0.0	0.0	0.0	0.0

Ca is assumed an artifact due to atmospheric dust contamination.

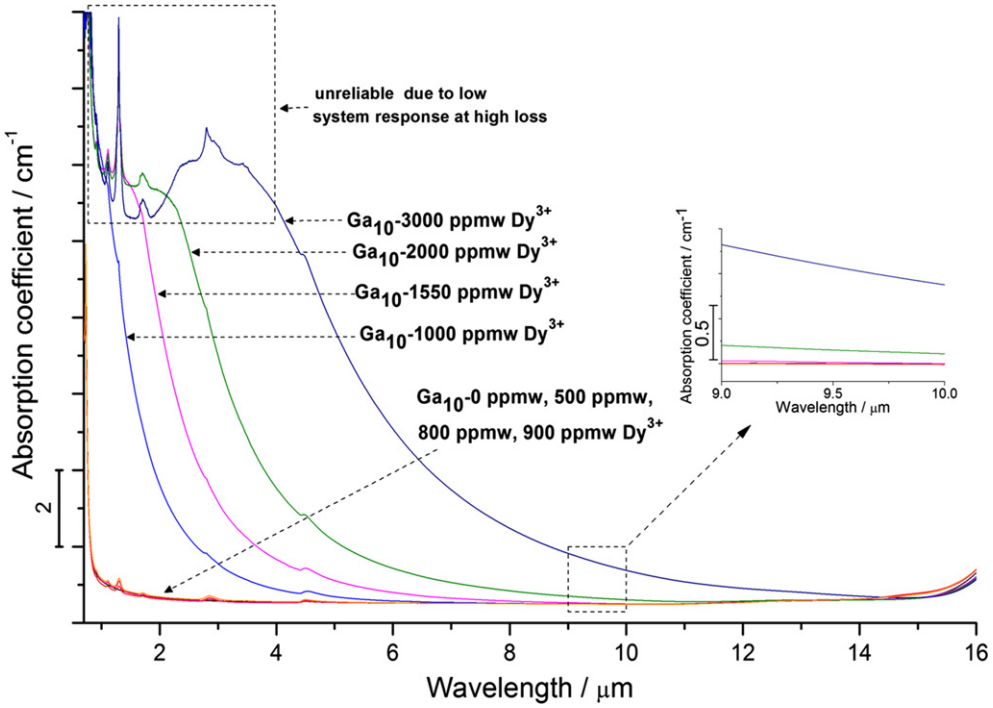

Fig. 10. FTIR spectra of the 0–3000 ppmw Dy^{3+}($DyCl_3$)-doped $Ge_{16.5}As_9Ga_{10}Se_{64.5}$ glasses. Inset shows the 9.0–10.0 μm wavelength region which is associated with the SiO_2 impurity band Si–O[34,35].

(including 1550 and 2000 ppmw Dy^{3+}-doped Ga_{10} FTIR spectra,[27] for comparison), respectively. It was assumed that the host glass samples exhibited no scattering (or minimal scattering due to careful polishing) and all spectra have been normalized to the host-glass (0 ppmw Dy^{3+}) baseline in order to highlight the excess scattering loss of Dy^{3+}-doped glasses over the undoped host glass. The sample surface quality (e.g., flatness and finish) produced a small variation (~0.04 absorption coefficient cm^{-1}) in the baseline in the near-IR region.

For all glasses there was no excess scattering until 1000 ppmw of the added Dy^{3+} dopant was reached; thereafter, the excess scattering increased with added Dy^{3+} and the return to zero scattering was at successively longer wavelengths.

From the inset in Fig. 10 and the inset (a) in Fig. 11, and for all of the glasses, no vibrational absorption at 9–10 μm wavelength[34,35] due to Si–O was observed (see insets, Figs. 10 and 11). This suggests that SiO_2 was not the primary scattering particle. Compared to [Si–O] chemical bond vibrational absorption, [Dy-O] has longer wavelength vibrational absorption due to the heavier vibrating mean mass and its absorption signature would therefore be masked by longer wavelength matrix oxide absorption bands beyond 12 μm.[36] Evidence for Dy_2O_3 formed in the bulk of Dy^{3+}-doped glasses has been presented here (Section 3.2: Figs. 5 and 6 and Table II). Although the added concentration of Dy^{3+} (≤0.3 wt%) was low, nevertheless the large difference in refractive index between Dy_2O_3 (1.97 at 589.3 nm)[37] and the chalcogenide glass matrix (~2.56 at 3 μm) implies a low threshold for onset of Rayleigh and Mie scattering for nanoparticles of Dy_2O_3.[38]

When compared to Si–O, [Si–O–Dy] could also have longer wavelength absorption due to the heavier element incorporation of Dy. Earlier it was shown that there was an increase in [Si–O–Dy] at the surface of glasses with increase in the added level of Dy^{3+} particles coming from the stronger ampoule corrosion by the higher concentration of $DyCl_3$ additive (Section 3.3). Besides, the scattering threshold of Ge-modified α-Ga_2Se_3 crystals could be far higher that of particulate Dy_2O_3 due to the much more closely matched refractive indices of Ge-modified α-Ga_2Se_3 crystals (~2.43 at 0.9 μm for annealed films[39]) and the host glass matrix (~2.56 at 3 μm).

We concluded from earlier work,[27] that the increase in the excess scattering found when increasing Dy^{3+} doping from 1000 to 2000 ppmw in Ga_{10} glasses in Fig. 10 was caused by an increase in the number or size of scattering centers due to the Ge-modified α-Ga_2Se_3 crystal and/or [Si–O–Dy] species found in the corroded glass surfaces. However, XRD patterns of Ga_{10} glasses (Section 3.1, Fig. 2) showed no real increase in the Ge-modified α-Ga_2Se_3 phase between 2000 and 3000 ppmw added Dy^{3+}. Therefore, in the case of 2000–3000 ppmw Dy^{3+}-doped Ga_{10} glasses, we suggest that the increased scattering scatter was caused by the increased Dy_2O_3 and [Si–O–Dy].

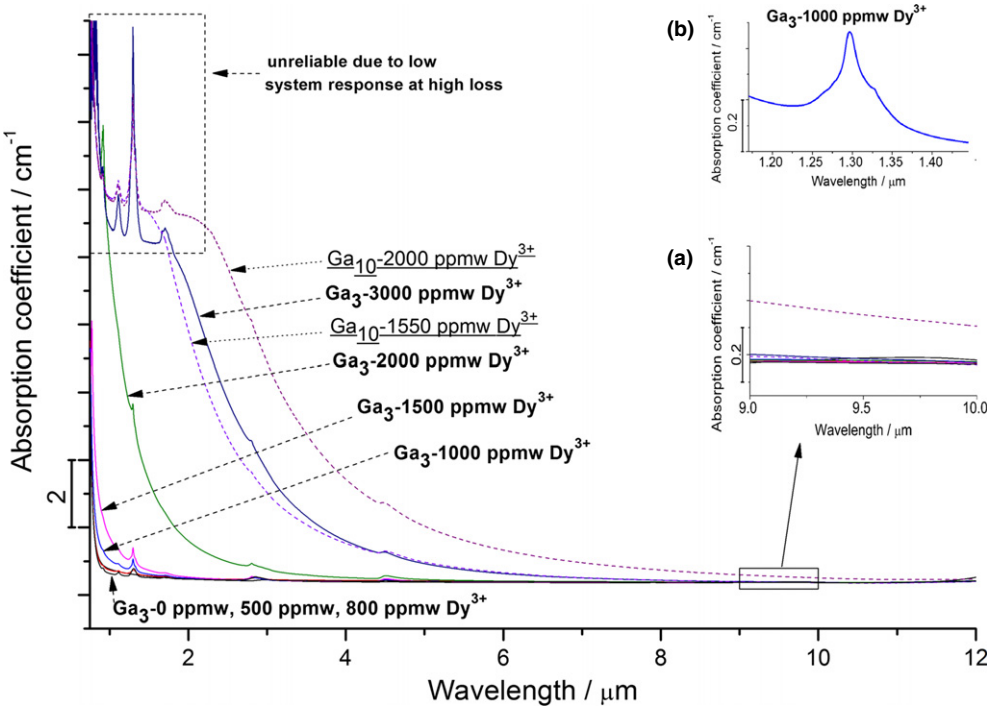

Fig. 11. Fourier transform infrared spectrometry spectra of 0–3000 ppmw Dy^{3+}($DyCl_3$)-doped $Ge_{16.5}As_{16}Ga_3Se_{64.5}$ glasses with two Ga_{10} series glasses as reference, 1550 and 2000 ppmw Dy^{3+}($DyCl_3$)-doped $Ge_{16.5}As_9Ga_{10}Se_{64.5}$ glasses. Inset (a) shows the 9.0–10.0 μm wavelength region associated with the SiO_2 impurity band Si–O.[34,35] Inset (b) presents an example of structuring of Dy^{3+} absorption band for ≥1000 ppmw Dy^{3+}-doped Ga_3 and Ga_{10} glasses.

In Fig. 11, the extra scattering loss found in the spectra of the Dy^{3+}($DyCl_3$)-doped Ga_3 glasses *pro rata* with Dy doping level is much lower than that for the Dy^{3+}($DyCl_3$)-doped Ga_{10} glasses. Although Ge-modified α-Ga_2Se_3 crystals were found by HRTEM (Section 3.2, Fig. 4), from XRD (Section 3.1, Fig. 3), the Ga_3 glasses were XRD amorphous. Thus, in the case of Ga_3 glasses, we propose that the excess scatter in the bulk glass is due to particulate Dy_2O_3, in addition to [Si–O–Dy] species and very small amount of Ge-modified α-Ga_2Se_3 crystals in the bulk glass.

Finally, at higher doping levels, for both Dy^{3+}($DyCl_3$)-doped Ga_3 and Ga_{10} glasses, the Dy^{3+} absorption band became structured when the Dy^{3+} concentration was ≥1000 ppmw (see inset (b) in Fig. 11 for an example spectrum). This phenomenon must be caused by a more ordered environment of the Dy^{3+} ions[4] and is subject of further investigation.

IV. Conclusions

When the Ga content was decreased from 10 to 3 at.% for Dy^{3+}($DyCl_3$)-doped $Ge_{16.5}As_{(19-x)}Ga_xSe_{64.5}$ glasses, XRD was unable to detect any crystallization on melt cooling. HRTEM, however, revealed rather isolated (difficult to find) nanocrystal clusters of the same Ge-modified *fcc* α-Ga_2Se_3 found most prevalent in heavily Dy^{3+}-doped, as-prepared, 10 at.% Ga glasses. For the first time, imaging and analytical HRTEM indicated that within one area less than 10 nm in diameter in the bulk glass there was a very high (two orders of magnitude greater than added) Dy concentration accompanied by a high, but nonquantifiable, [O] concentration and these were within the same region as Ga_2Se_3 nanocrystals in a bulk of an as-annealed Dy^{3+}-doped Ga_3 glass. Although this was an isolated sighting, nevertheless it provides a rationale for the overall observed behavior. Thus, it is proposed that Dy^{3+}, the most electropositive species in the glassmelt scavenges adventitious [O] the most electronegative species in the melt, present as a contaminant. The resulting Dy_2O_3 has similar unit cell lattice registry to the crystallizing Ge-modified *fcc* α-Ga_2Se_3 phase and hence is an energetically favorable heterogeneous nucleating agent. FTIR revealed excess light scattering of the Dy^{3+}-doped Ga_3 glass series was much lower than for the Ga_{10} glass series. The main reason was the reduced quantity and size of the Ge-modified α-Ga_2Se_3 crystals found in the bulk of the Dy^{3+}-doped Ga_3 glass series. But it is important to point out that the scattering threshold (i.e., particle size and density) is far lower for Dy_2O_3 (and [Si–O–Dy]) than for the Ge-modified *fcc* α-Ga_2Se_3 phase due to the greater mismatch of refractive index with the glass matrix. FTIR and HRTEM found no evidence for Si–O species in the bulk of melts. Roughened areas of spot defects on Ga_3 and Ga_{10} glass surfaces that had been in contact with the silica glass ampoule containment during melt cooling were found to contain Dy, Si, and [O] contamination.

Being glasses, the chalcogenides may be shaped to fiber. However, if the RE dopant becomes oxidized, likely to occur during glassmelting, and if this RE oxide acts as the heterogeneous nucleating agent for bulk crystal growth during melt cooling, then not only is the host matrix transparency compromised, in terms of excess light scattering but also the absorption and emission cross sections of the rare-earth ion are compromised.[4] This is because that part of the population of RE ions bound in a high phonon–energy oxide local environment will be inactive as a mid-IR fluorophores, undergoing preferential nonradiative decay of RE-ion excited states. To be able to optimize the RE-ion concentration without paying any penalty of RE-ion oxidation and/or increased devitrification in the preform or fiber are vital steps toward realizing the fabrication of MIR fiber lasers.

References

[1]L. B. Shaw, B. Cole, P. A. Thielen, J. S. Sanghera, and I. D. Aggarwal, "Mid-Wave IR and Long-Wave IR Laser Potential of Rare-Earth Doped Chalcogenide Glass Fiber," *IEEE Quant. Electron.*, **37** [9] 1127–37 (2001).

[2]B. Cole, L. B. Shaw, P. C. Pureza, R. Mossadegh, J. S. Sanghera, and I. D. Aggarwal, "Rare-Earth Doped Selenide Glasses and Fibers for Active Applications in the Near and Mid-IR," *J. Non-Cryst. Solids*, **256–257**, 253–9 (1999).

[3]M. Pollnau and S. Jackson, "Mid-Infrared Fiber Lasers"; pp. 225–61 in *Solid-State Mid-Infrared Laser Sources*, Vol. 89, Edited by I. Sorokina and K. Vodopyanov. Springer Verlag Berlin, 2003.

[4]A. B. Seddon, Z. Tang, D. Furniss, S. Sujecki, and T. M. Benson, "Progress in Rare-Earth-Doped Mid-Infrared Fiber Lasers," *Opt. Express*, **18** [25] 26704–19 (2010).

[5]M. Ebrahim-Zadeh, and I. Sorokina, *Mid-Infrared Coherent Sources and Applications*. Springer, the Netherlands, 2005.

[6]J. S. Sanghera, L. B. Shaw, and I. D. Aggarwal, "Chalcogenide Glass-Fiber-Based Mid-IR Sources and Applications," *Quant. Electron.*, **15** [1] 114–9 (2009).

[7]X. Zhu and N. Peyghambarian, "High-Power Zblan Glass Fiber Lasers: Review and Prospect," *Adv. Optoelectron*, **2010**, 1–23 (2010).

[8]F. Prudenzano, L. Mescia, L. A. Allegretti, M. De Sario, T. Palmisano, F. Smektala, V. Moizan, V. Nazabal, and J. Troles, "Design of Er^{3+}-Doped Chalcogenide Glass Laser for Mid-IR Application," *J. Non-Cryst. Solids*, **355** [18–21] 1145–8 (2009).

[9]F. Prudenzano, L. Mescia, L. Allegretti, V. Moizan, V. Nazabal, and F. Smektala, "Theoretical Study of Cascade Laser in Erbium-Doped Chalcogenide Glass Fibers," *Opt. Mater.*, **33** [2] 241–5 (2010).

[10]R. S. Quimby, L. B. Shaw, J. S. Sanghera, and I. D. Aggarwal, "Modeling of Cascade Lasing in Dy^{3+} Chalcogenide Glass Fiber Laser with Efficient Output at 4.5 Microns," *Photon. Technol. Lett.*, **20** [2] 123–5 (2008).

[11]S. Sujecki, L. Sójka, E. Bereś-Pawlik, Z. Tang, D. Furniss, A. Seddon, and T. Benson, "Modelling of a Simple Dy^{3+} Doped Chalcogenide Glass Fibre Laser for Mid-Infrared Light Generation," *Opt. Quant. Electron.*, **42** [2] 69–79 (2010).

[12]N. P. Barnes and R. E. Allen, "Room Temperature Dy:YLF Laser Operation at 4.34 μm," *IEEE J. Quant. Electron.*, **27** [2] 277–82 (1991).

[13]M. C. Nostrand, R. H. Page, S. A. Payne, and W. F. Krupke, "Room-Temperature Laser Action at 4.3-4.4 μm in $GaGa_2S_4$:Dy^{3+}," *Opt. Lett.*, **24** [17] 1215–7 (1999).

[14]P. Němec and M. Frumar, "Compositional Dependence of Spectroscopic Parameters of Dy^{3+} Ions in Ge-Ga-Se Glasses," *Mater. Lett.*, **62** [17–18] 2799–801 (2008).

[15]Z. Tang, D. Furniss, M. Fay, N. C. Neate, S. Sujecki, T. M. Benson, and A. B. Seddon, "Crystallisation and Optical Loss Studies of Dy^{3+}-Doped, Low Ga Content, Selenide Chalcogenide Bulk Glasses and Optical Fibers"; pp. 193–9 in *Processing, Properties, and Applications of Glass and Optical Materials: Ceramic Transactions*, Vol. 231. Edited by A. K. Varshneya, H. A. Schaeffer, K. A. Richardson, M. Wightman and L. D. Pye. John Wiley & Sons, Inc., Hoboken, NJ, 2012

[16]Z. Tang, D. Furniss, S. Sujecki, T. M. Benson, and A. B. Seddon, "The Effect of the Nature of the Rare Earth Additive on Chalcogenide Glass Stability"; pp. 79121F in *Proceedings of the SPIE, Solid State Lasers XX: Technology and Devices.*, Vol. 7912, Edited by W. A. Clarkson, N. Hodgson and R. Shori. SPIE, Bellingham, WA, 2011

[17]Y. Cheng, Z. Tang, N. C. Neate, D. Furniss, T. M. Benson, and A. B. Seddon, "The Influence of Dysprosium Addition on the Crystallization Behavior of a Chalcogenide Selenide Glass Close to the Fiber Drawing Temperature," *J. Am. Ceram. Soc.*, **95** [12] 3834–41 (2012).

[18]P. Němec, M. Frumar, B. Frumarová, M. Jelínek, J. Lančok, and J. Jedelský, "Pulsed Laser Deposition of Pure and Praseodymium-Doped Ge-Ga-Se Amorphous Chalcogenide Films," *Opt. Mater.*, **15** [3] 191–7 (2000).

[19]S. Kasap, K. Koughia, G. Soundararajan, and M. G. Brik, "Optical and Photoluminescence Properties of Erbium-Doped Chalcogenide Glasses (Gegas: Er)," *Quant. Electron.*, **14** [5] 1353–60 (2008).

[20]M. F. Churbanov, I. V. Scripachev, V. S. Shiryaev, V. G. Plotnichenko, S. V. Smetanin, E. B. Kryukova, Y. N. Pyrkov, and B. I. Galagan, "Chalcogenide Glasses Doped with Tb, Dy and Pr Ions," *J. Non-Cryst. Solids*, **326–327**, 301–5 (2003).

[21]M. S. Iovu, N. N. Syrbu, Y. S. Tveryanovich, and G. J. Adriaenssens, "Photoluminescence of $Ga_{0.016}Ge_{0.25}As_{0.083}S_{0.65}$ Glasses Doped with Rare-Earth Ions," *J. Optoelectron. Adv. M*, **8** [4] 1341–4 (2006).

[22]V. Lyubin, M. Klebanov, B. Sfez, M. Veinger, R. Dror, and I. Lyubina, "Photoluminescence, Photostructural Transformations and Photoinduced Anisotropy in Rare-Earth-Doped Chalcogenide Glassy Films," *J. Non-Cryst. Solids*, **352** [9–20] 1599–601 (2006).

[23]Y. Choi and J. Song, "Spectroscopic Properties of Tm^{3+} Ions in Chalcogenide Ge-As-S Glass Containing Minute Amount of Ga and CsBr," *Opt. Commun.*, **281** [17] 4358–62 (2008).

[24]T. Schweizer, B. N. Samson, J. R. Hector, W. S. Brocklesby, D. W. Hewak, and D. N. Payne, "Infrared Emission From Holmium Doped Gallium Lanthanum Sulphide Glass," *Infrared Phys. Technol.*, **40** [4] 329–35 (1999).

[25]L. B. Shaw, B. Cole, D. T. Schaafsma, B. B. Harbison, J. S. Sanghera, and I. D. Aggarwal, "Rare-Earth-Doped Selenide Glass Optical Sources"; pp. 420–1 in Proceedings of Lasers and Electro-Optics. Cleo 98, Technical Digest, Optical Society of America, Washington, DC, 1998.

[26]L. Sojka, Z. Tang, H. Zhu, E. Beres-Pawlik, D. Furniss, A. B. Seddon, T. M. Benson, and S. Sujecki, "Study of Mid-Infrared Laser Action in Chalcogenide Rare Earth Doped Glass with Dy^{3+}, Pr^{3+} and Tb^{3+}," *Opt. Mater. Express*, **2**, 1580–7 (2012).

[27]Z. Tang, N. C. Neate, D. Furniss, S. Sujecki, T. M. Benson, and A. B. Seddon, "Crystallization Behavior of Dy^{3+}-Doped Selenide Glasses," *J. Non-Cryst. Solids*, **357** [11–13] 2453–62 (2011).

[28]B. G. Aitken, C. W. Ponader, and R. S. Quimby, "Clustering of Rare Earths in GeAs Sulfide Glass," *C. R. Chim.*, **5** [12] 865–72 (2002).

[29]J. K. Kim, B. K. Jin, W. J. Chung, B. J. Park, J. Heo, and Y. G. Choi, "Influence of the Ga Addition on Optical Properties of Pr in Ge-Sb-Se Glasses," *J. Phys. Chem. Solids*, **72** [11] 1386–9 (2011).

[30]T. H. Lee, S. I. Simdyankin, J. Hegedus, J. Heo, and S. R. Elliott, "Spatial Distribution of Rare-Earth Ions and GaS_4 Tetrahedra in Chalcogenide Glasses Studied Via Laser Spectroscopy and Ab Initio Molecular Dynamics Simulation," *Phys. Rev. B*, **81** [10] 1042041–6 (2010).

[31]T. Lee, S. Simdyankin, L. Su, and S. Elliott, "Evidence of Formation of Tightly Bound Rare-Earth Clusters in Chalcogenide Glasses and Their Evolution with Glass Composition," *Phys. Rev. B*, **79** [18] 1802021–4 (2009).

[32]R. Jing, Y. Guang, Z. Huidan, Z. Xianghua, Y. Yunxia, and C. Guorong, "Properties of Dy^{3+}-Doped Ge-As-Ga-Se Chalcogenide Glasses," *J. Am. Ceram. Soc.*, **89** [8] 2486–91 (2006).

[33]P. Lucas, A. A. Wilhelm, M. Videa, C. Boussard-Plédel, and B. Bureau, "Chemical Stability of Chalcogenide Infrared Glass Fibers," *Corros. Sci.*, **50** [7] 2047–52 (2008).

[34]M. Churbanov, "High-Purity Chalcogenide Glasses as Materials for Fiber Optics," *J. Non-Cryst. Solids*, **184**, 25–9 (1995).

[35]W. A. King, A. G. Clare, and W. C. Lacourse, "Laboratory Preparation of Highly Pure As_2Se_3 Glass," *J. Non-Cryst. Solids*, **181**, 231–7 (1995).

[36]C. T. Moynihan, P. B. Macedo, M. S. Maklad, R. K. Mohr, and R. E. Howard, "Intrinsic and Impurity Infrared-Absorption in As_2Se_3," *J. Non-Cryst. Solids*, **17**, 369–85 (1975).

[37]O. Medenbach, D. Dettmar, R. D. Shannon, R. X. Fischer, and W. M. Yen, "Refractive Index and Optical Dispersion of Rare Earth Oxides Using a Small-Prism Technique," *J. Opt. A*, **3** [3] 174–7 (2001).

[38]P. France, "Critical Reports on Applied Chemistry"; pp. 188–204, *Fluoride Glasses*, Vol. 27, Edited by A. E. Comyns. Society of the Chemical Industry, John Wiley & Sons, Chichester, 1989

[39]M. A. Afifi, A. E. Bekheet, H. T. El-Shair, and I. T. Zedan, "Determination and Analysis of Optical Constants for Ga_2Se_3 Films Near Absorption Edge," *Phys. B*, **325**, 308–18 (2003). □